Quantum Homodyning of Photonic Qubits, Qutrits and Ququads Emitted on Demand from an Atomic Source

Peter B. R. Nisbet-Jones, Jerome Dilley, Annemarie Holleczek, Oliver Barter, and Axel Kuhn*
University of Oxford, Clarendon Laboratory, Parks Road, Oxford, OX1 3PU, UK
(Dated: March 1, 2013)

Quantum information processing (QIP) has become an attractive interdisciplinary research topic [1]. With single quantum systems controlled to encode elementary 'quantum' bits (qubits) of information, a fundamental enhancement of computing and information security is now in reach [2, 3]. Particular attention is paid to QIP in linear-optics quantum circuits (LOQC) [4–7], which are in principle scalable to larger networks if it were not for the spontaneous nature of parametric down conversion (PDC) photon sources. Here, we demonstrate that single photons deterministically emitted from a single atom into an optical cavity [8–10] can be equally used for LOQC, thus levying these restrictions. With a $\sim$ 500 ns coherence time, also a sub-dividision of photons into several time bins of arbitrary amplitudes and phases is possible. In particular, in place of storing a simple qubit in one photon (being present or absent), the subdivision into *d* time bins is now used to encode arbitrary qu*d*its in one photon. We verify the fidelity of the encoding with a series of quantum-homodyne measurements. These are performed by sending the photons of interest together with single reference photons (acting as local oscillator) into a small quantum network consisting of one single beam-splitter, and monitoring the photon-photon correlations between its output ports in a time resolved manner [11, 12].

One of the most challenging tasks in LOQC is preparing the initial quantum states of the photons. This is typically achieved via dual-rail entanglement [13] where a single photon incident on a 50:50 beam-splitter is split between the two output ports into the non-separable state

$$|\Psi\rangle = \frac{1}{\sqrt{2}}\left(|10\rangle + e^{i\phi}|01\rangle\right), \qquad (1)$$

which is the general representation of a photon prepared in a quantum superposition of two modes, whether these occupy different regions in space, or separate periods in time. Here, we concentrate on the latter – for a twin-peak photon in time, we may associate the amplitude of $|10\rangle$ with the probability of detecting the photon in the the first peak, and the amplitude of $|01\rangle$ with the probability of detecting it in the second peak. In case the amplitudes and the relative phase ϕ between the two peaks (or time bins) can be freely adjusted, such a photon may represent any arbitrary qubit.

We achieve this desired degree of flexibility using a strongly coupled atom-cavity source to efficiently generate photons of almost any arbitrary amplitude and phase evolution [9, 10]. Fig. 2a shows that we have a single ^{87}Rb atom coupled to a high-finesse cavity undergoing a Raman transition between two hyperfine ground states. This transition – driven by a pump laser $\Omega(t)$ and the vacuum field of the cavity mode [14] – results in the emission of a single photon through the output coupling mirror of the cavity. The amplitude of the driving laser is modulated such that N-peak photons of 230 ns peak duration are obtained. Fig. 2b shows the intensity of twin-peak and triple peak photons of 460 ns and 680 ns duration, respectively. To impose an arbitrary phase change of ϕ between neighbouring peaks within one photon, it is sufficient to alter the phase of the driving laser between peaks. This is accomplished with a phase shift to the radio frequency controlling the acousto-optic modulator we use to generate the driving pulse. Thus even the creation of more complex states is trivial, as we can directly shape the amplitude and phase profile of the photons. The photon source exhibits a very high emission probability of 85 % [15], singleness ($g^2(0) < 0.05$), and operates at a repetition rate of 1 MHz.

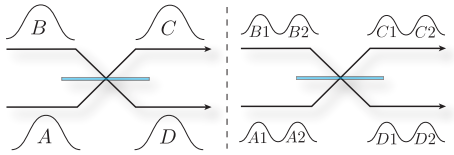

FIG. 1. Quantum homodyning of single- and twin-peak photons. Photons of identical envelope arrive simultaneously. The local-oscillator photon exhibits no internal phase jumps, but the signal does. This gives rise to correlation events.

To fully verify that the quantum state of the emitted photons corresponds to the desired qubits, we need to monitor their phase with time, or at least measure the relative phase between individual time bins. We do this with a newly developed quantum homodyning technique. In contrast to the continuous variable regime [16], it is not based on the interference between a strong 'classical' local oscillator (LO) and a weak signal beam, but relies only on quantum interference. The signal photon defined by Eq. (1) interferes on a beam splitter (BS) with a single LO photon, $|\Psi_{LO}\rangle = \left(|10\rangle + |01\rangle\right)/\sqrt{2}$, which exhibits no

* axel.kuhn@physics.ox.ac.uk

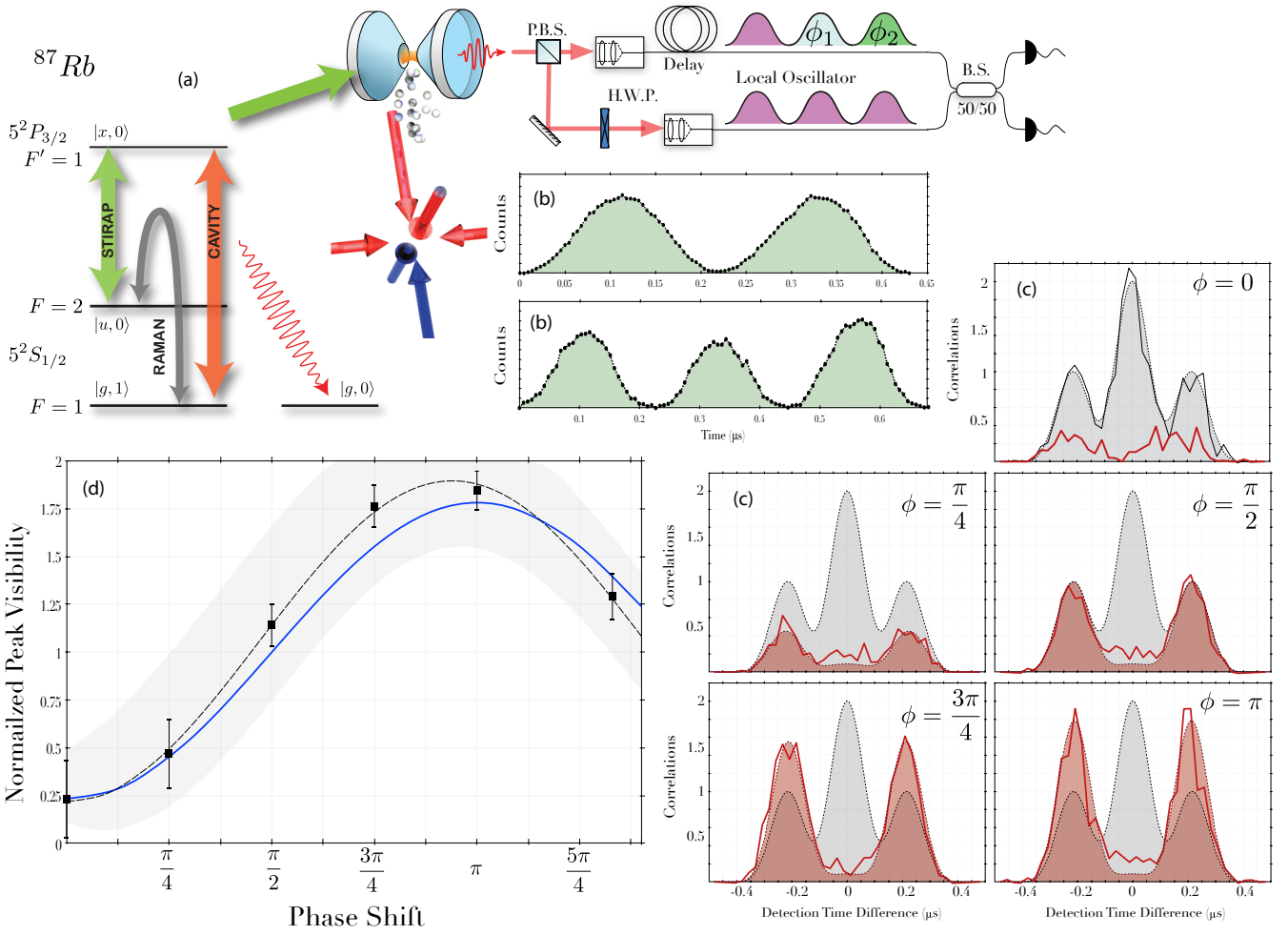

FIG. 2. Single-photon source. **(a)** A single ^{87}Rb atom is placed inside a high-finesse cavity using an atomic fountain. A Raman transition is driven within this atom which produces a single photon with a pre-determined spatio-temporal envelope, for example of double or triple-peak shape. A 200 m long fibre is used to delay one photon such that it overlaps with the subsequently emitted photon. **(b)** Intensity envelope of twin-peak and triple-peak photons. **(c)** Cross-correlation function from the homodyne measurement of twin-peak photons as a function of detection time delay τ. The reference signal (perpendicular polarisation) is shown in grey, the homodyne signal (parallel polarisations) is red. The relative phase shift ϕ between the signal-photon peaks has been varied from 0 to π. **(d)** Visibility of the cross-correlation side peaks (see text) shown along with the expected dependence (blue) and the 95 % confidence bounds (grey).

phase shift between time bins. Fig. 1 shows that the photons arrive simultaneously at the BS in spatio-temporal modes A and B, thus that the input state $\hat{a}^\dagger_A\hat{a}^\dagger_B|0\rangle$ translates into a superposition of output states using the operator relation of the BS, $\hat{a}^\dagger_{A,B} \propto \hat{a}^\dagger_C \pm \hat{a}^\dagger_D$. Applied to twin-peak signal and LO photons, the unnormalised creator of the output state reads

$$(\hat{a}^\dagger_{C1})^2 - (\hat{a}^\dagger_{D1})^2 + e^{i\phi}\Big((\hat{a}^\dagger_{C2})^2 - (\hat{a}^\dagger_{D2})^2\Big) + \tag{2}$$

$$\Big((\hat{a}^\dagger_{C1}\hat{a}^\dagger_{C2} - \hat{a}^\dagger_{D1}\hat{a}^\dagger_{D2})(1+e^{i\phi}) \tag{3}$$

$$-(\hat{a}^\dagger_{C2}\hat{a}^\dagger_{D1} - \hat{a}^\dagger_{D2}\hat{a}^\dagger_{C1})(1-e^{i\phi})\Big), \tag{4}$$

where the indices 1 and 2 refer to the corresponding time bins. The first line contains all the creation operator pairs where both photons are detected in the same time-bin. Here the photons always coalesce and are found in the same output port. The more interesting final lines describe the situation where the photons are detected in different time-bins. In the case of identical photons ($\phi = 0$) the cross terms vanish and no correlations between different detectors are found. This corresponds to the well known Hong-Ou-Mandel effect [17]. However, if we choose $\phi = \pi$ the photons do not always coalesce, instead they are actively forced into opposite output ports if detected in different time bins. For instance, with the first photon detected in $C1$, the second *must* be detected in $D2$. The photon correlations, which normally follow

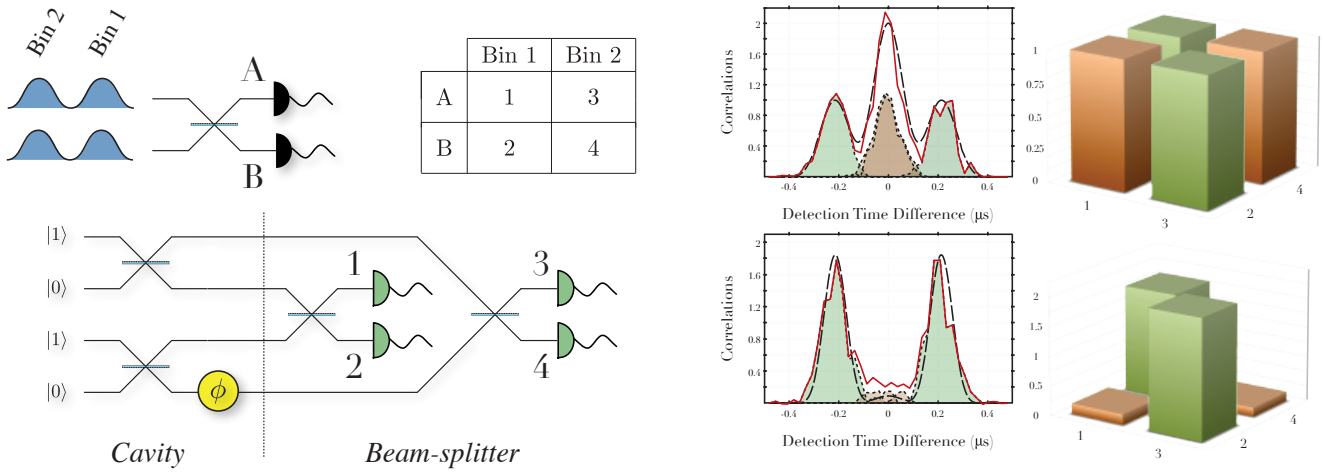

FIG. 3. Equivalent photonic circuits: The emission of two twin-peak photons and their subsequent time-resolved overlap on a beam-splitter is represented as an equivalent quantum circuit using spatial modes. Real time-resolved detector clicks can be mapped to virtual detectors firing using the translation table. Correlations from the time-resolved quantum-homodyne signal can be sub-divided into cases where both detectors fire in the same time bin (brown), or in successive time bins (green). The signal thus reduces to the correlations between virtual detectors, shown as 3D bar charts. The upper plots are for perpendicularly polarized photons and the lower for parallel photons with a $\phi = \pi$ phase shift.

bosonic statistics, are projected into a quasi-fermionic state by the first detection and the change in relative phase. Thus the photons do not coalesce if detected in different time-bins. Therefore, by examining the number of correlations in opposite ports of the beamsplitter, the value of the relative phase difference between any pair of time-bins can be determined.

A simplified outline of the experimental arrangement along with the cross correlation of the two single-photon detectors is shown in Fig. 2a. The stream of alternating signal and LO photons is emitted from the cavity and split equally by a polarizing beamsplitter (PBS) between the long (upper) and short (lower) beam paths, thus that successively emitted signal and LO photons may arrive simultaneously at the non-polarising 50:50 beam splitter (BS). When perpendicularly polarized the photons do not interfere and the correlation function is the auto-convolution of the photon shape, i.e. a triple peak in case of twin-peak photons, (grey in 2c), with a large central peak caused by detector clicks in $\hat{a}^\dagger_{C1}\hat{a}^\dagger_{D1}$ and $\hat{a}^\dagger_{C2}\hat{a}^\dagger_{D2}$ and two side peaks of half the height caused by the correlations between $\hat{a}^\dagger_{C1}\hat{a}^\dagger_{D2}$ and $\hat{a}^\dagger_{C2}\hat{a}^\dagger_{D1}$.

With parallel polarization the photons interfere and the correlation function (red) depends strongly on the relative phase between the two peaks of the signal photon. As discussed above, no correlations are found within identical time bins, so the central peak around zero detection-time delay vanishes. This is not the case for the two side peaks in the correlation function centred around ± 230 ns. These can be attributed to correlations between the two detectors with photons registered in different time bins. The number of these events depends strongly on ϕ and is expected to vary between zero and twice the number of reference counts (those of the perpendicular-polarised photons).

The visibility [18] of the cross-correlation side peaks at ± 230 ns is shown as a function of ϕ in Fig. 2d. The data clearly shows the expected behaviour; starting from a minimum at $\phi = 0$ the correlations rise to a maximum with at $\phi = \pi$ and then decrease again. It does not span the full $0 \rightarrow 2$ range due to the inherent coherence time of the experiment (500 ns). Taking the latter into account, the expected change in peak visibility has been calculated (blue trace). It agrees well with a theoretical fit to the data (grey, confirmed within the 95 % confidence bounds of a χ^2-test).

A better insight is gained by drawing an equivalent quantum circuit, where different time bins are sketched as if they were different spatial modes (Fig. 3). In reality, we have two photons, each existing in both time bins, and all interfering on a single beam-splitter with detectors A and B in its output ports. The successive production of the twin-peak photons in the cavity corresponds to sending single photons to a beam splitter, with a possible phase shift in one of the signal-photon modes. Outside the cavity, the real beam splitter is used twice (once per time bin), and so are the detectors. Hence the equivalent outside circuit consists of two virtual beamsplitters and four virtual detectors. As we can allocate all photon counts to their specific time bins, a simple translation table can be drawn to map the real detector clicks to the corresponding virtual detectors firing. It is a straightforward exercise to link cross correlations between these virtual detectors to the correlation pattern shown in Fig. 2(c). These can be thought of as the sum of the four possi-

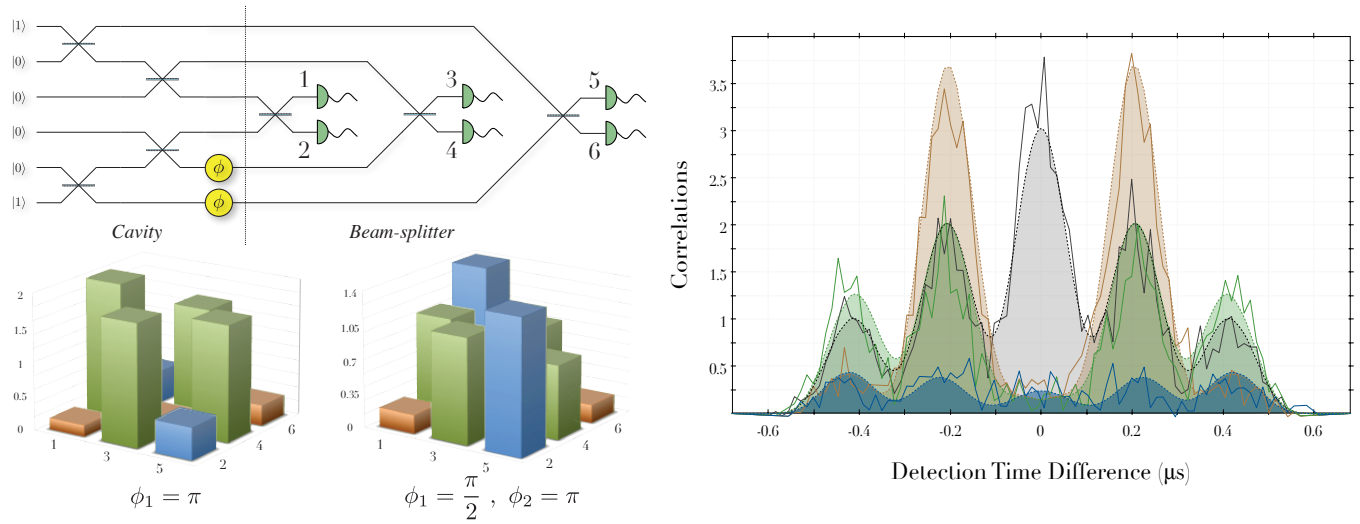

FIG. 4. Qutrits: With the number of time-bins increased to three, the quantum circuit substantially increases in size. There are now seven beam-splitters and six detectors in the virtual setup whilst the apparatus is unchanged. The right-hand plot shows the time-resolved correlations for photons with perpendicular polarisation (grey) and parallel polarized photons (blue) with a phase shift in the central time-bin of $\phi_1 = \pi$ (orange) and with phase shifts of $\phi_1 = \pi/2$ in the central and $\phi_2 = \pi$ in the final time bins (green). The correlations of the virtual detectors are also shown as 3D bar charts.

ble detector cross-correlations, $C_{1,2}, C_{3,4}$ and $C_{1,4}, C_{2,3}$. However, as we record the absolute time at which the real detectors fire, all virtual correlations can be defined. This is shown for both perpendicularly polarized photons and parallel polarized photons with a $\phi = \pi$ phase shift in the signal photon. The full time-resolved correlation function – which might depend strongly on the photon shape – can therefore be time-binned and normalized to give the relative correlations between virtual detectors. Using these, the fidelity of the qubit state preparation was found to be $F = 0.93$.

So far, we have shown that it is possible to use time-bin encoding to represent a photonic qubit. However, the versatile photon-generation process does not limit us to twin-peak photons. We can scale up the system, adding additional time-bins, each with their own amplitude and and arbitrary relative phases between them. In other words we can produce arbitrary qudits. To demonstrate this scaling ability we have produced triple-peak photons, corresponding to the state:

$$|\Psi\rangle = |100\rangle + e^{i\phi_1}|010\rangle + e^{i\phi_2}|001\rangle \qquad (5)$$

The equivalent circuit which illustrates the preparation and analysis of this qutrit is shown in Fig. 4. Although the physical apparatus remains unchanged, the virtual circuitry has greatly expanded; we now mimic six detectors using the two which are bolted to our laser table. The correlations for the qutrit photons are shown in Figure 4, both as a time-resolved quantum-homodyne signal and as correlations between the six virtual detectors. The photon-photon correlation rates found between the various time bins (1-2, 2-3, 1-3) all depend on the relative phases as expected. Hence encoding a qutrit in a single photon is as straightforward as expected. The increase in number of time bins is limited only by the coherence time and the intrinsic evolution rates of the photon production $(g, \kappa) = 2\pi \cdot (15, 12)$ MHz. Within these limits, we even managed to go one step further in encoding ququads in photons consisting of four well-separate time bins. With these, we still control the relative phases between various time bins. However, the visibility of cross-correlations between the first and the last time bin is slightly reduced, as the period spanned by four time bins exceeds the coherence time.

Finally, we would like to point out that we initialise all time bins upon photon generation. In contrast to various other approaches [19, 20], this new mechanism is inherently loss-free and also has the potential of mapping superposition states between atoms and time-binned photons [21]. Furthermore, albeit the narrow photonic bandwidth, we fully control their phase and mutual coherence properties, so that the criteria set in [22] for optimal LOQC photons do not really apply. In particular, the rather slow photon generation process and the otherwise small photonic circuits and fast detectors allow for feedback during photon generation – for instance, the geometrical length of the photons is far longer than the distance from source to detector. Thus with twin-peak photons and a phase flip conditioned on what detector fires in the first time bin, we can control to which detector the second photon goes, provided it gets detected in the second time bin. This level of control is unprecedented in single-photon applications.

In conclusion, for all measurements presented here, we have found that the time-resolved analysis of the measured quantum-homodyne signal beautifully coincides

with the theoretical predictions. This demonstrates that we successfully prepare deterministically produced photons in arbitrary quantum states, i.e. qubits and qutrits, with efficiencies of up to 85 % and fidelities > 90 %. As a single atom is able of emitting more than 100 times prior to leaving the optical cavity, the present achievements pave the way to large-scale photonic quantum networks, with an effective complexity further enhanced by the number of well-separated and therefore resolvable time bins realised within one photon.

ACKNOWLEDGMENTS

This work was supported by the Engineering and Physical Sciences Research Council (EP/E023568/1), the Deutsche Forschungsgemeinschaft (Research Unit 635), and the EU through the RTN EMALI (MRTN-CT-2006-035369).

[1] M. A. Nielsen and I. L. Chuang, *Quantum Computation and Information* (Cambridge University Press, 2000).
[2] D. P. DiVincenzo, Fortschr. Phys. **48**, 771 (2000).
[3] T. D. Ladd, F. Jelezko, R. Laflamme, Y. Nakamura, C. Monroe, and J. L. O'Brien, Nature **464**, 45 (2010).
[4] E. Knill, R. Laflamme, and G. J. Milburn, Nature **409**, 46 (2001).
[5] T. C. Ralph, A. G. Witte, W. J. Munro, and G. J. Milburn, Phys. Rev. A **65**, 012314 (2001).
[6] P. Kok, W. J. Munro, K. Nemoto, T. C. Ralph, J. P. Dowling, and G. J. Milburn, Rev. Mod. Phys. **79**, 135 (2007).
[7] J. L. O'Brien, Science **318**, 1567 (2007).
[8] A. Kuhn and D. Ljunggren, Contemp. Phys. **51**, 289 (2010).
[9] G. S. Vasilev, D. Ljunggren, and A. Kuhn, New Journal of Physics **12**, 063024 (2010).
[10] P. B. R. Nisbet-Jones, J. Dilley, D. Ljunggren, and A. Kuhn, New J. Phys. **13**, 103036 (2011).
[11] T. Legero, T. Wilk, M. Hennrich, G. Rempe, and A. Kuhn, Phys. Rev. Lett. **93**, 070503 (2004).
[12] T. Legero, T. Wilk, A. Kuhn, and G. Rempe, Adv. At. Mol. Opt. Phys. **53**, 253 (2006).
[13] T. Pittman, B. Jacobs, and J. Franson, Phys. Rev. Lett. **88**, 257902 (2002), quant-ph/0109128.
[14] A. Kuhn, M. Hennrich, and G. Rempe, Phys. Rev. Lett. **89**, 067901 (2002).
[15] For strongly coupled atoms, a maximum detection efficiency of 20 % is found. Taking the detector efficiencies, fibre-coupling losses and cavity losses into account, this corresponds to an intra-cavity photon generation efficiency of 85 %.
[16] H. P. Yuen and V. W. S. Chan, Opt. Lett. **8**, 177 (1983).
[17] C. K. Hong, Z. Y. Ou, and L. Mandel, Phys. Rev. Lett. **59**, 2044 (1987).
[18] The visibility is defined by the ratio of quantum-homodyne correlations to the number of perpendicular-polarised reference correlations.
[19] I. Marcikic, H. de Riedmatten, W. Tittel, V. Scarani, H. Zbinden, and N. Gisin, Phys. Rev. A **66**, 062308 (2002).
[20] H. P. Specht, J. Bochmann, M. Mücke, B. Weber, E. Figueroa, D. L. Moehring, and G. Rempe, Nature Photonics **3**, 469 (2009).
[21] J. Dilley, P. Nisbet-Jones, B. W. Shore, and A. Kuhn, Phys. Rev. A **85**, 023834 (2012).
[22] P. P. Rohde, T. C. Ralph, and M. A. Nielsen, Phys. Rev. A **72**, 052332 (2005).